GRIM-19 mutations fail to inhibit v-Src-induced oncogenesis

Sudhakar Kalakonda[£], **Shreeram C. Nallar**[£], **Daniel J. Lindner**[$], **Peng Sun**, **Robert R. Lorenz**[¶], **Eric Lamarre**[¶], **Sekhar P. Reddy**[**], and **Dhananjaya V. Kalvakolanu**[*]

Department of Microbiology & Immunology, Program in Oncology, Greenebaum Cancer Center, University of Maryland School of Medicine, Baltimore, MD 21201

[$]Taussig Cancer Center, Cleveland Clinic Foundation, Cleveland, OH 44195

[¶]Head & Neck Institute, Cleveland Clinic Foundation, Cleveland, OH 44195

[**]Department of Pediatrics, College of Medicine, University of Illinois at Chicago, Chicago, IL 60612

Abstract

The non-receptor tyrosine kinase Src is a major player in multiple physiological responses including growth, survival and differentiation. Overexpression and/or oncogenic mutation in the *Src* gene have been documented in human tumors. The v-Src protein is an oncogenic mutant of Src, which promotes cell survival, migration, invasion and division. *GRIM-19* is an anti-oncogene isolated using a genome-wide knockdown screen. GRIM-19 binds to transcription factor STAT3 and ablates its pro-oncogenic effects while v-Src activates STAT3 to promote its oncogenic effects. However, we found that GRIM-19 inhibits the pro-oncogenic effects of v-Src independently of STAT3. Here, we report the identification of functionally inactivating *GRIM-19* mutations in a set of Head and Neck cancer patients. While wild-type GRIM-19 strongly ablated v-Src-induced cell migration, cytoskeletal remodeling and tumor metastasis, the tumor-derived mutants ($L^{71}P$, $L^{91}P$ and $A^{95}T$) did not. These mutants were also incapable of inhibiting the drug resistance of v-Src-transformed cells. v-Src down regulated the expression of Pag1, a lipid raft-associated inhibitor of Src, which was restored by wild-type GRIM-19. The tumor-derived mutant GRIM-19 proteins failed to upregulate Pag1. These studies show a novel mechanism that deregulates Src activity in cancer cells.

Keywords

Tumor suppression; Oncogenes; Cytoskeleton; Metastasis; Cytokines

[*]Corresponding author: 410-328-1396, dkalvako@umaryland.edu.
[£]Contributed equally to this study.

Conflict of Interest statement: The authors declare no conflicts of interests.

Introduction

The Src family of non-receptor protein tyrosine kinases (SFKs) regulates a number of cellular processes including growth factor and immune receptor signaling, metabolic responses, cell survival, and cell motility (1). The v-Src (viral) and c-Src (cellular) proteins differ in their carboxyl termini, with the former lacking 11 of the c-terminal most amino acids that fold to form an auto-inhibitory domain (1). Constitutive phosphorylation of a tyrosine residue in this region, Y^{530} (human)/Y^{535} (rodent) by the C-terminal Src kinase (Csk), renders the enzyme inactive. Dephosphorylation of this tyrosine residue sets the stage for autophosphorylation of Y^{419} (human)/Y^{424} (rodent), in the kinase domain and a super-activation of its kinase function (1). As a result, v-Src escapes the negative regulation by Csk (2). v-Src phosphorylates a number of proteins associated with plasma membrane, cytoskeleton, adherens junctions, proteins involved in cell migration, invasion, proliferation, survival and transcription machinery (1).

Earlier, we employed a genome-wide knockdown screen and discovered the Genes-associated with Retinoid-IFN induced Mortality (GRIM), which conferred a growth advantage to cells following their knockdown (3). GRIM-19 was one such gene product, whose overexpression caused growth arrest and/or apoptosis (4). One of the major targets of GRIM-19 is transcription factor STAT3 (5, 6). STAT3 is transiently activated *via* tyrosyl phosphorylation by the Janus tyrosine kinases (JAKs) which are recruited to the cytokine-engaged receptors (7). In tumors, STAT3 is constitutively phosphorylated by activated/mutated oncogenic tyrosine kinases, such as v-src (8, 9). Under these conditions, STAT3 induces the expression of many gene products involved in promoting cell growth, invasion and suppression of apoptosis (10). We have shown earlier that GRIM-19 inhibits v-Src-induced cellular transformation (11), involving remodeling of actin cytoskeleton in a STAT3-independent manner (12).

Here, we describe three functionally inactivating somatic mutations in the *GRIM-19* gene from primary human oral squamous cell carcinoma (SCC), which unlike the wild type were inefficient at suppressing v-Src-induced cellular transformation, tumor growth, cytoskeletal remodeling and metastatic behavior. The v-Src oncoprotein suppressed the expression level of lipid raft-associated protein Cbp/Pag1; an inhibitor of Src. Wild-type GRIM-19 overrode v-Src-induced repression of Pag1 and rescued Pag1 levels thereby enforcing growth suppression. The tumor-derived GRIM-19 mutants failed to rescue Pag1 levels. These results identify a novel anti-oncogene regulatory mechanism and its deregulation in cancers.

Results

Identification of mutations in GRIM-19 gene from human oral SCC

We recently obtained a set of human oral SCC samples from individuals who were long-term tobacco users. Total RNA and genomic DNA were isolated from pathologist-certified surgically isolated tumors and adjacent normal tissues. Real-time PCR analyses showed *GRIM-19* mRNA levels in some of the tumors was higher compared to their matched normal tissue (Fig. 1A). Since GRIM-19 was an inhibitor of cell growth, we were surprised by this inverse correlation between its expression and tumor formation. Sequencing of *GRIM-19*

cDNA from tumors and matched normals identified three separate base changes in the GRIM-19 mRNA from tumors (Fig. S1). Their somatic origin was ascertained by a genomic sequence comparison from a matched normal tissue. These *GRIM-19* mutants were from patients with poorly differentiated lymph node metastases. These mutants $L^{71}P$, $L^{91}P$ and $A^{95}T$ were cloned into expression vectors to determine their biological effects on v-Src-induced oncogenesis.

GRIM-19 mutants fail to block v-Src-induced cellular transformation

To study the biological effects, GRIM-19 (mutants and wild type) expression vectors were transfected into 3Y1 cell line that stably expressed v-Src. After verifying their comparable expression (Fig. 1B), we analyzed their effect on v-Src-induced anchorage independent growth in soft agar medium. Control vector-transfected 3Y1 cells (EV) did not form significant colonies (>25 μm diameter) while v-Src-expressing cells formed large sized colonies (ranging from 90μm to 1mm) (Fig. 1C). In the presence of wild-type GRIM-19, fewer colonies formed with an average colony diameter ~70μm. In the presence of mutant GRIM-19 proteins, v-Src promoted the formation of several large colonies (200μm to 900μm). Thus, all three GRIM-19 mutants failed to inhibit anchorage-independent growth like wild-type GRIM-19 (Fig. 1D).

GRIM-19 mutants are incapable of blocking v-Src-induced cell motility

We next tested if these GRIM-19 mutants had any differential effect on v-Src-dependent motility using a wound scratch model. Confluent monolayers of cells expressing v-Src and GRIM-19 were scratched to generate a denuded area in the monolayer to permit cell movement. A large number of v-Src-expressing cells moved into the denuded area by 4h, compared to the control vector (EV) transfected cells (Fig. 2A). Such motility was ablated in the presence of wild-type GRIM-19. All three mutants significantly (*p*<0.001) lost their ability to block v-Src-induced motility compared to wild-type GRIM-19 (Fig. 2B). The $L^{71}P$ and $A^{95}T$ mutants nearly lost all of their capacity to block v-Src in this assay while $L^{91}P$ mutant was intermediary between wild-type GRIM-19 and v-Src.

GRIM-19 mutants do not block v-Src-dependent glucose consumption

Since most rapidly growing cancer cells utilize glucose for biosynthetic processes, we wanted to determine if GRIM-19 had an effect on glucose metabolism. Equal numbers of cells expressing v-Src in the absence and presence of GRIM-19 proteins were grown in DMEM (high glucose) for 72h and select parameters were assayed in the spent medium. Glucose levels depleted strongly in media from v-Src-expressing cells, which was significantly (*p*<0.01) suppressed in presence of wild-type GRIM-19 (Fig. 3A). The mutants, however, were unable to prevent glucose depletion. Low glucose levels in the medium correlated inversely with lactic acid levels (Fig. 3B). The v-Src-induced rise in lactic acid levels was well controlled by wild-type GRIM-19 but not by the mutants. These metabolic alterations also reflected in corresponding changes in pH of the growth medium (Fig. 3C). In light of these observations, we checked for the presence and levels of pyruvate kinase (PK) isoforms M1 and M2 in these cells using qPCR. M1 is seen in most adult cells while M2 is expressed mainly during embryogenesis. Expression of PKM2 isoform was correlated with a

shift towards increased glycolysis and transformed state of cells (13). In these cells, only *Pkm2* transcript was found (see below). When compared to EV, the v-Src-expressing cells had a significant increase in *Pkm2* levels, which was lowered by wild-type GRIM-19 (Fig. 3D). The mutant GRIM-19 proteins were unable to suppress *Pkm2* transcript levels like the wild type. *Pkm2* transcript levels in mutant-expressing cells were comparable to that of v-Src-expressing cells. Since an invariant PCR primer was used in this analysis, we ensured that the product observed in these reactions contained only *Pkm2* by performing a restriction analysis. The Xho I and Sfo I restriction enzymes sites, present in the alternate exon 9, are specific to *Pkm1* and *Pkm2* transcripts, respectively (Fig. 3E left panel). The product was digested only by Sfo I but not by Xho I (Fig. 3E right panel). The Kpn I digestion served as marker to show that the product is indeed *Pkm*.

Tumor-derived GRIM-19 mutants cannot restrain v-Src-induced cytoskeletal remodeling

Most normal cells retain a well-spread shape when attached to a substratum, which could be observed in the parental 3Y1 cell line. Although adherent, a greater number of v-Src-transformed cells appeared rounded under light microscope (Fig. S2). Such a change is required for motility and invasion, by disrupting actin stress fibers. As reported in our earlier study (12), expression of wild-type GRIM-19 reverted the cell shape of v-Src-transformed 3Y1 cells similar to that of naive 3Y1 cells. Unlike this, mutant-expressing cells appeared more like v-Src-expressing cells. Therefore, we next examined the influence of GRIM-19 and tumor-derived mutants on cytoskeletal reorganization caused by v-Src. Phalloidin staining revealed that in control vector-transfected cells, only actin stress fibers were seen, while in v-Src-expressing cells, they were completely absent and actin localized to discrete lamellipodium-filopodium-like structures or densely to rosette-like structures resembling podosomes (Fig. 4A). In the presence of wild-type GRIM-19, a moderate levels of stress fibers reappeared with a decline in lamellipodium-filopodium-like structures (Fig. 4A). In contrast, mutant-expressing cells had a complete absence of actin stress fibers with several lamellipodium-filopodium-like structures. Similar data were observed when cells were stained with cortactin (Fig. S3). The ability of the same GRIM-19 mutants to affect cytoskeletal organization was also examined in an oral squamous cell carcinoma cell line, HSC3, which expresses a very low level of GRIM-19. Similar to the observations in 3Y1 cells, expression of wild-type GRIM-19 suppressed lamellipodium-filopodium-like structures in HSC3 cells (Fig. S4). The mutants, however, lost such ability. Taken together, these observations show that GRIM-19 ablates v-Src-induced cytoskeletal reorganization and tumor-derived mutants are incapable of exerting such effects.

Since v-Src induces the phosphorylation of multiple cellular proteins involved in cytoskeletal organization, we investigated if GRIM-19 blocked these events to retain a normal cell shape. Western blot analyses with antibodies that could detect site-specific tyrosyl phosphorylation in proteins involved in cell adhesion and F-actin regulation, FAK, paxillin and cortactin, showed a significant increase in their tyrosyl phosphorylated levels in v-Src-expressing cells, compared to control vector transfected ones. In presence of wild-type GRIM-19, these three proteins were not phosphorylated to a high level (Fig. 4B). In contrast, all three mutants lost the capacity to block v-Src-mediated phosphorylation of FAK, paxillin and cortactin (Fig. 4B). The $L^{71}P$ mutant was completely ineffective at

blocking phosphorylation of FAK or cortactin or paxillin, which was either comparable or higher than v-Src-expressing cells while mutants $L^{91}P$ and $A^{95}T$ moderately inhibited v-Src activity. Thus, among the mutants a differential inhibition of v-Src activity was evident and even the strongest GRIM-19 mutant was still far less efficient compared to wild-type GRIM-19. Lastly, GRIM-19 mutants also failed block src-induced tyrosylphosphorylation of transcription factor STAT3 and gene expression (Fig. S5), unlike the wild-type protein.

GRIM-19 mutants failed to suppress v-Src-induced growth and metastatic spread of tumor cells

To address if the mutants lost the capacity to suppress tumor growth *in vivo*, nude mice were injected with v-Src-transformed cells co-expressing GRIM-19 (wild type or mutants). At the end of four weeks, differences in tumor size among the mutants were clearly observed ($L^{71}P > L^{91}P > A^{95}T$) that were much bigger compared to wild-type GRIM-19 which continued till the end of seven weeks (Fig. 5A). These differences were highly significant ($p<0.001$). Thus, the mutants were incapable of suppressing v-Src-induced tumor growth *in vivo*. Next, we addressed if these mutants influenced metastasis. Cells expressing v-Src and GRIM-19 were transduced with a lentiviral vector expressing fire-fly luciferase and injected subcutaneously in the lower flank of nude mice. Metastatic spread of cells was monitored using a live imaging system. Control vector-transfected cells did not grow or move from the site of injection while v-Src-expressing cells grew and spread to adjacent areas (Fig. 5B). Wild-type GRIM-19-expressing cells grew slightly but did not spread like v-Src-expressing cells. Metastases were mostly located in the retroperitoneum, with lower frequencies in the vertebral bodies, liver and spleen. The $L^{71}P$ and $L^{91}P$ mutants, on other hand, failed to block metastatic spread of cells to different parts of the body. The most robust cell spread was observed with cells expressing v-Src/$L^{71}P$ followed by v-Src/$L^{91}P$. The $A^{95}T$ expressing cells moved weakly compared to the other two GRIM-19 mutants, consistent with its relatively better growth-suppressive effects compared to the other mutants (Fig. 5C).

Mechanism of the anti-v-Src effects of GRIM-19

To define mechanism(s) of the anti-Src effects of wild-type GRIM-19, we first assessed Y^{416}-Src phosphorylation in cells expressing v-Src and GRIM-19. As expected, tyrosyl phosphorylation of Src was readily seen in v-Src-expressing cells compared to the EV cells (Fig. 6A). Active Src (Y^{416}-phosphorylation) levels were the lowest in wild-type GRIM-19-expressing cells, while they were highest in $L^{71}P$ mutant-expressing cells followed by $A^{95}T$ and $L^{91}P$. Thus, the increased tyrosyl phosphorylation of Src substrates in presence of GRIM-19 mutants (see Figs. 4 and S5) appears to be due to a failure to block v-Src kinase activity. Initial experiments did not provide evidence for a direct interaction between GRIM-19 and v-Src (data not shown). Therefore, we hypothesized that GRIM-19 might activate the expression of a Src inhibitor and the mutants were incapable of doing so.

A CSK-binding protein associated with lipid rafts (Cbp/Pag1) could independently suppress v-Src activity as shown by an increased susceptibility of *Pag1*$^{-/-}$ MEFs to v-Src-induced transformation (14). Therefore, we examined if v-Src affected *Pag1* expression level and a role for GRIM-19 in this process. Real-time PCR analysis revealed a strong reduction in *Pag1* mRNA level in the presence of v-Src (Fig. 6B), which was restored to near normal

levels in presence of wild-type GRIM-19. The mutants on the other hand failed to counter the repressive effect of v-Src on *Pag1* expression levels. Thus, *Pag1* appears to act as a GRIM-19-responsive v-Src inhibitor to suppress tumor cell growth. Consistent with the qPCR data, v-Src suppressed Pag1 protein levels. Such repression was countered by wild-type GRIM-19 and increased it above the Pag1 levels found in EV cells (Fig. 6C). To ascertain the role of GRIM-19 in the upregulation of Pag1, we transduced v-Src/GRIM-19 expressing cells with lentiviral particles coding for either scrambled or GRIM-19-specific shRNA (*sh-G*). After ensuring the specific depletion of GRIM-19 by *sh-G* (Fig. 6D), we examined if Pag1 levels were affected using a Western blot analysis. Indeed, depletion of wild-type GRIM-19 lead to a decline in Pag1 levels, similar to those found in v-src transformed cells (Fig. 6E). As expected, depletion of the mutants using the same approach did not significantly alter Pag1 levels, because Pag1 is already low in these cells. Consistent with the loss of GRIM-19 and the consequent loss of Pag1 levels, v-src activity rose up, that was reflected by a rise in the tyrosyl phosphorylation of FAK (Fig. 6F). The biological relevance of these observations was ensured by measuring cell motility using a Transwell migration assay (Fig. 6G). As expected higher numbers of v-src transformed cells rapidly moved to the bottom side of the Transwell chambers (where mitogens are present) when compared to the EV cells. In presence of GRIM-19 cell motility is blocked strongly, which was reversed following the knockdown of GRIM-19 (Fig. 6G). Similar knockdown in mutant expressing cells did not significantly alter cell motility. Taken together these data indicate an important role for GRIM-19 in maintaining PAG1 levels to blunt v-src activity.

Lastly, to determine the relevance of Pag1 to GRIM-19 mediated inhibition of v-Src, we knocked down Pag1 using a specific shRNA (*sh-Pag1*), expressed from a lentiviral vector. We used v-Src and v-Src/WT cell lines for this study (Fig. 6H). The *sh-Pag1* knocked down the expression of Pag1 >82%, compared to the *sh-Scr* control in the v-Src/WT cells. As Pag1 is undetectable in presence of v-Src alone, *sh-Pag1* did not affect it in the v-Src cells. Following the loss of Pag1, v-Src activity and FAK1 phosphorylation were significantly increased in v-Src/WT cells. Fig. 6I shows the quantified data from the Western blots. Lastly, the v-Src/WT ells acquired the capacity to form soft-agar colonies in presence of *sh-Pag1*, compared to the control (Fig. 6J–K). As expected, *sh-Pag1* did not affect colony formation in the v-Src cells. Thus, loss of either GRIM-19 or Pag1 produced a similar stimulatory effect on v-Src activity in these cells, indicating a major role for Pag1 in mediating anti-Src activity of GRIM-19.

Discussion

The Src proto-oncogene is hyperactivated either due to mutation/over expression or due to constitutive activity of mutated growth factor receptors (1). Src plays a critical role in cell survival (15) and bone metastasis of certain cancers (16) by phosphorylating multiple cellular proteins involved in survival, motility, invasion and cytoskeletal organization. Src activity in normal cells is restrained by a protein tyrosine kinase Csk that phosphorylates the c-terminal $Y^{530/535}$ residue (2, 17, 18).

As mentioned earlier, GRIM-19 inhibits transcription factor STAT3 (5). We and others have shown that GRIM-19 (RNA and protein) expression is down regulated in a variety of human

primary tumors compared to their matched normal tissue, including kidney (19), prostate (20), cervical (21), lung (22), gastro-intestinal (23) and brain (24) cancers. Here we described inactivating *GRIM-19* mutations in SCC. Public databases (NCBI and ENSEMBL) have many entries for SNPs in *GRIM-19* linked to a sequencing project at the Johns Hopkins University, although no disease annotations are available. Interestingly, mutations in codons (71 and 91 for leucine) described in this study, are also found in these public databases. Both these mutations have lost their ability to block v-Src. These residues are conserved in *GRIM-19* of human, mouse, rat, cow and *Xenopus* probably indicating an important function. Together, these mutations define a potential domain within GRIM-19 required for exerting anti-metastatic functions.

Compared to wild-type GRIM-19, the mutants displayed moderate to severe loss of anti-tumor functions (Figs. 2–5). Despite some quantitative differences, the net effect was as inability to block v-Src induced growth *in vivo*. Importantly, these mutants could not restore actin stress fibers and failed to block anchorage-independent growth. Focal adhesions typically contain integrins, Fak, Src and actin-anchoring proteins which are necessary for cell migration (25). Podosomes are actin-rich cell membrane protrusions that play a role in cell motility (26). Clustering of podosomes result in rosette-like or belt-shaped structures associated with extracellular matrix-degrading protease activity (26). Many invasive cancer cells display both these features in addition to high levels of active Src and phosphorylated FAK. An important actin regulator in podosomes is cortactin. Cortactin has a higher affinity for the nodes in a branched actin network (27, 28). Upon phosphorylation by Src, cortactin loses such affinity allowing actin to be remodeled by other regulators. A high level of phosphorylated cortactin is seen in invasive gastro-intestinal tumors along with high levels of active Src and phosphorylated FAK often associated with a poor prognosis (29). Cortactin is frequently over expressed in a number of metastatic tumors (28, 30, 31) and particularly in a high percentage of primary aggressive oral SCCs (32). Within the head and neck squamous carcinomas, Src/FAK overexpression is associated with poor prognosis (33, 34). In Betel-Quid induced oral squamous cell carcinoma, src activation plays prominent in tumor cell invasion (35). In other experimental models, combined treatment of HNSCC with SFK and EGFR inhibitor yielded better tumor suppression, indicating an important role for Src in tumor growth (36). Therefore, the metastatic behavior of v-Src-expressing cells (Fig. 6) and a critical role played by GRIM-19 in controlling cancer growth can be envisaged in light of these reports. GRIM-19 blocked v-Src-mediated tyrosyl phosphorylation of cortactin, a critical event in the remodeling of the actin network. This is a transcription-independent event given there was no change in total *Cttn* levels (data not shown) under the conditions of either v-Src or v-Src/GRIM-19 expression. Thus, GRIM-19 alters post-translational events involved in cortactin function. We have shown earlier that the anti-Src effects of GRIM-19 are exerted independently of STAT3 (12). The growth patterns of v-src/GRIM-19 mutants are also consistent with relatively higher glucose uptake, compared to wild-type GRIM-19 protein under the same conditions *in vitro* (Fig. 3). It has been shown earlier that Src can induce the expression of glucose transporters and hexokinases (37–39). Together these data show a broader effect of GRIM-19 on v-Src-induced oncogenic alterations. Most advanced tumor cells depend heavily on aerobic glycolysis (40) to meet their high energy demands. One change that corresponds to the inefficient glucose

metabolism in these cells is the rise in *Pkm2* transcript following v-Src expression, which was suppressed by wild type, but not by the mutant GRIM-19 proteins. Interestingly, these cells did not express *Pkm1* transcript at all, indicating that in 3Y1 cells PKM2 is the only source of PK.

Since a v-Src/GRIM-19 complex could not be detected, we hypothesized that GRIM-19 might engage an inhibitory protein for suppressing v-Src activity. Although the first suspect would be Csk, v-Src lacks its target site and cannot explain the inhibitory effects of GRIM-19. A novel Src inhibitory mechanism operates through a protein called Csk-binding protein (Cbp), also known as phosphoprotein associated with glycosphingolipid-enriched microdomains 1 (Pag1). Interaction of Pag1-Csk, in lipid rafts, promoted Src inactivation by phosphorylating $Y^{530/535}$ residue. (41). This is an attractive mechanism but cannot explain anti-v-Src effects of GRIM-19, because it lacks $Y^{530/535}$. However, a recent study has shown that Cbp/Pag1 itself inhibits Src activity independently of Csk (14). Cbp binds to the SH2 domain of active Src and arrests it in lipid rafts to prevent its oncogenic effects. The $Pag1^{-/-}$ MEFs are readily transformed by v-Src, which can be suppressed by complementing with Pag1 expression. Importantly, *CBP/PAG1* mRNA is down regulated in tumor cells expressing active Src (14). Consistent with the latter observation, we observed a down regulation of *Pag1* in v-Src-expressing 3Y1 cells, which was regained in presence of wild-type GRIM-19 (Fig. 6) but not in presence of the mutant GRIM-19. RNA*i*-mediated knockdown of either GRIM-19 or Pag1 in cells expressing v-Src/GRIM-19 resulted in a resumption of v-Src activity, tyrosyl phosphorylation of FAK and increased cell motility and soft-agar colony formation. These observations are consistent with their lack of control over v-Src and a failure to restore Pag1 expression. In summary, Pag1 re-expression in presence of GRIM-19 appears to be a potential mechanism of v-Src inhibition. A portion of GRIM-19 is also present mitochondrion(42), where it appears to control electron transport chain I activity (43), which could generate reactive oxygen species (44). SFK activity is also regulated by redox control mechanisms through cysteine oxidation (45). Whether redox activities also contribute to the anti-src activities of GRIM-19, remains to be investigated.

v-Src neither affected *Pag1* mRNA stability nor the luciferase activity driven by Pag1 promoter in their experiments, which we were able to confirm (data not shown). Recently, the v-Src, Ha-Ras and Ki-Ras oncoproteins were reported to suppress Pag1 gene expression through a MAP kinase-dependent histone deacetylation (46). Although a role for HDAC1 is suggested in the *Pag1* repression (46), the exact nuclear factors targeted by v-src are still unknown. It is likely that GRIM-19 blocks such processes for upregulating Pag1, given its nuclear presence (4). There are no known STAT3 binding sites in the *Pag1* promoter (data not shown) to suggest that STAT3 inhibits *Pag1* transcription and GRIM-19 reverses it. Furthermore, we have shown that GRIM-19 inactivation of v-Src activity occurs independently of STAT3 (12). Future studies are required to resolve the factors targeted by v-Src in repressing *Pag1* and how GRIM-19 affects them. A similar negative regulation of *Pag1* occurred in presence of EGF and PDGF(46). Based on these observations, we believe that GRIM-19 operates a negative regulatory loop by restoring Pag1 levels which block the oncogenic effects of v-Src. Lastly, cells expressing v-Src are highly resistant to inhibition by chemotherapeutics, which was blunted in cells expressing GRIM-19. Mutant GRIM-19

proteins, described here, were unable to block v-Src-induced chemoresistance suggesting their pathological importance (data not presented). These GRIM-19 mutants may serve as guides to co-treat tumors harboring them with Src inhibitors in addition to standard chemotherapeutics, to achieve an optimal suppression. However, a systematic large-scale analysis of the relevance of the mutations reported here to human primary oral SCC diagnosis and therapy is still required, which is beyond the scope of current study.

Materials and Methods

Reagents

Primary antibodies specific for Myc tag, Src, phospho-Y^{416} Src, STAT3, phospho-Y^{705} STAT3, cortactin, phospho-Y^{421} cortactin, paxillin, phospho-Y^{118} paxillin (Cell Signaling Technology); Fak, phospho-$Y^{576-577}$ Fak (Upstate Biotechnology); β-actin (Sigma-Aldrich); Pag1 (Abcam, Inc) were used in these studies. Secondary antibodies against anti-mouse and anti-rabbit IgG conjugated with Alexa Fluor 750 and 700 (Invitrogen), respectively were used in Western blots (Odyssey system, LICOR) or Immunoprecipitation (IP) or Immunofluorescence (IF) analyses.

SCC samples

Samples were collected after informed consent under an institutionally approved protocol at the Cleveland Clinic Foundation, Cleveland, OH. Total RNA from tumors and matched normal tissues was converted to cDNA and used for PCR with gene-specific primers (Table S1). The PCR products were sequenced at the University of Maryland Biopolymer/ Genomics core facility, Baltimore, MD. The corresponding base changes were verified by sequencing the PCR products of genomic DNA with specific primers (Table S2).

Cell lines and plasmids

An immortalized non-oncogenic rat fibroblast cell line (3Y1), was grown in DMEM containing 10% FBS. Expression vectors for v-Src and Myc epitope-tagged wild-type GRIM-19 are described in our previous studies (11) and transfected cells were selected with G418 (Calbiochem) and puromycin (Sigma-Aldrich), respectively, for stable expression. Sequencing-confirmed *GRIM-19* mutants from SCC samples were cloned into lentiviral expression vector pLVX-Puro (Clontech Inc) to express as a Myc epitope-tagged protein. Primers used for cloning *GRIM-19* ORF are shown in Table S1. Expression-positive cell pools (>50 colonies per transfection) were used to generate stable population that were used in all experiments. Lentiviral expression vectors coding for GRIM-19- and Cbp/Pag1-specific shRNAs were obtained from Open Biosystems, Inc. A scrambled shRNA expression vector was used as a control in each case. Lentiviral particles expressing either the shRNAs or the GRIM-19 mutants were generated as described in our earlier publications.

Immunofluorescence

To visualize F-actin network and nuclei, Alexa Fluor 555-conjugated phalloidin (Invitrogen) and DAPI (Sigma-Aldrich) were used, respectively. GRIM-19 (wild type and mutants) were visualized by indirect immunofluorescence using anti-Myc IgG. Images were captured using

a fluorescence microscope (Olympus BX-FLA) fitted with a digital camera (QICAM) and processed by Q-capture pro 5.1 (Q-Imaging Corporation). Cortactin and $pY^{41}6$-Src were detected using AF-555 and AF-488 tagged secondary antibodies, respectively.

Cell growth, motility and gene expression analyses

In vitro growth, wound healing, Boyden (Transwell) migration, and soft-agar colony formation assays were performed as described in our previous reports (11). Real-time PCR analyses were performed with specific primers (Table S3) using JumpStart SYBR Green Master Mix (Sigma-Aldrich) in a Stratagene Mx3005P real time PCR machine. Expression differences of specific transcripts were quantified using the *RPL32* or *ACTB* as the internal controls by the CT method. Western blot analyses were performed using the LI-COR Odyssey infrared imager (LI-COR Biotechnology, Lincoln, NE) and the intensities of bands of interest were quantified using the software provided by the manufacturer and normalized to internal control.

Tumorigenic assays

These experiments were performed as described earlier (47) under an IACUC approved protocol. Cells (2×10^6 cells/mouse) expressing various combinations of GRIM-19 and v-Src were inoculated into the flank of NCr nu/nu mice (n=10/group) and growth was measured over a period of several weeks. To monitor the metastatic spread, these cells were Lentivirally transduced to express fire-fly luciferase. Nude mice (n=6/group) were injected on the lower left flank with cells (10^5/mouse) subcutaneously. Animals were monitored for metastatic tumor spread using bioluminescence. Anaesthetized mice were imaged 5 min after an intraperitoneal administration luciferin (3mg/mouse) using the IVIS-100 Imaging System (Xenogen, Alameda, CA). Mice were placed on a heated shelf to maintain body temperature during the entire process. A seven-position filter wheel allowed imaging in different spectral ranges to measure depth and distribution of the emitted light *vis-à-vis* luciferase-expressing cells. Intensity of the emitted light is shown as a pseudocolor graphic over the black and white image of the animal.

Statistical analyses

All data were subjected to Student's *t*-test with p 0.05 considered significant.

Supplementary Material

Refer to Web version on PubMed Central for supplementary material.

Acknowledgments

References

1. Frame MC. Newest findings on the oldest oncogene; how activated src does it. Journal of cell science. 2004; 117:989–98. [PubMed: 14996930]

2. Superti-Furga G, Fumagalli S, Koegl M, Courtneidge SA, Draetta G. Csk inhibition of c-Src activity requires both the SH2 and SH3 domains of Src. The EMBO journal. 1993; 12:2625–34. [PubMed: 7687537]

3. Hofmann ER, Boyanapalli M, Lindner DJ, Weihua X, Hassel BA, Jagus R, et al. Thioredoxin reductase mediates cell death effects of the combination of beta interferon and retinoic acid. Mol Cell Biol. 1998; 18:6493–504. [PubMed: 9774665]

4. Angell JE, Lindner DJ, Shapiro PS, Hofmann ER, Kalvakolanu DV. Identification of GRIM-19, a novel cell death-regulatory gene induced by the interferon-beta and retinoic acid combination, using a genetic approach. J Biol Chem. 2000; 275:33416–26. [PubMed: 10924506]

5. Zhang J, Yang J, Roy SK, Tininini S, Hu J, Bromberg JF, et al. The cell death regulator GRIM-19 is an inhibitor of signal transducer and activator of transcription 3. Proc Natl Acad Sci U S A. 2003; 100:9342–7. [PubMed: 12867595]

6. Lufei C, Ma J, Huang G, Zhang T, Novotny-Diermayr V, Ong CT, et al. GRIM-19, a death-regulatory gene product, suppresses Stat3 activity via functional interaction. Embo J. 2003; 22:1325–35. [PubMed: 12628925]

7. Stark GR, Darnell JE Jr. The JAK-STAT pathway at twenty. Immunity. 2012; 36:503–14. [PubMed: 22520844]

8. Yu CL, Meyer DJ, Campbell GS, Larner AC, Carter-Su C, Schwartz J, et al. Enhanced DNA-binding activity of a Stat3-related protein in cells transformed by the Src oncoprotein. Science. 1995; 269:81–3. [PubMed: 7541555]

9. Bromberg JF, Horvath CM, Besser D, Lathem WW, Darnell JE Jr. Stat3 activation is required for cellular transformation by v-src. Mol Cell Biol. 1998; 18:2553–8. [PubMed: 9566875]

10. Yu H, Pardoll D, Jove R. STATs in cancer inflammation and immunity: a leading role for STAT3. Nat Rev Cancer. 2009; 9:798–809. [PubMed: 19851315]

11. Kalakonda S, Nallar SC, Gong P, Lindner DJ, Goldblum SE, Reddy SP, et al. Tumor suppressive protein gene associated with retinoid-interferon-induced mortality (GRIM)-19 inhibits src-induced oncogenic transformation at multiple levels. Am J Pathol. 2007; 171:1352–68. [PubMed: 17823279]

12. Sun P, Nallar SC, Kalakonda S, Lindner DJ, Martin SS, Kalvakolanu DV. GRIM-19 inhibits v-Src-induced cell motility by interfering with cytoskeletal restructuring. Oncogene. 2009; 28:1339–47. [PubMed: 19151760]

13. Mazurek S. Pyruvate kinase type M2: a key regulator of the metabolic budget system in tumor cells. Int J Biochem Cell Biol. 2011; 43:969–80. [PubMed: 20156581]

14. Oneyama C, Hikita T, Enya K, Dobenecker MW, Saito K, Nada S, et al. The lipid raft-anchored adaptor protein Cbp controls the oncogenic potential of c-Src. Molecular cell. 2008; 30:426–36. [PubMed: 18498747]

15. Byers LA, Sen B, Saigal B, Diao L, Wang J, Nanjundan M, et al. Reciprocal regulation of c-Src and STAT3 in non-small cell lung cancer. Clinical cancer research: an official journal of the American Association for Cancer Research. 2009; 15:6852–61. [PubMed: 19861436]

16. Zhang XH, Wang Q, Gerald W, Hudis CA, Norton L, Smid M, et al. Latent bone metastasis in breast cancer tied to Src-dependent survival signals. Cancer cell. 2009; 16:67–78. [PubMed: 19573813]

17. Sabe H, Hata A, Okada M, Nakagawa H, Hanafusa H. Analysis of the binding of the Src homology 2 domain of Csk to tyrosine-phosphorylated proteins in the suppression and mitotic activation of c-Src. Proceedings of the National Academy of Sciences of the United States of America. 1994; 91:3984–8. [PubMed: 7513429]

18. Nada S, Yagi T, Takeda H, Tokunaga T, Nakagawa H, Ikawa Y, et al. Constitutive activation of Src family kinases in mouse embryos that lack Csk. Cell. 1993; 73:1125–35. [PubMed: 8513497]

19. Alchanati I, Nallar SC, Sun P, Gao L, Hu J, Stein A, et al. A proteomic analysis reveals the loss of expression of the cell death regulatory gene GRIM-19 in human renal cell carcinomas. Oncogene. 2006; 25:7138–47. [PubMed: 16732315]

20. Liu YB, Shen WG, Ge H, Gai XD, Lu LL, Zhao XJ. Expressions of survivin and GRIM-19 in prostate cancer. Zhonghua nan ke xue = National journal of andrology. 2011; 17:21–6. [PubMed: 21351527]

21. Zhou Y, Li M, Wei Y, Feng D, Peng C, Weng H, et al. Down-regulation of GRIM-19 expression is associated with hyperactivation of STAT3-induced gene expression and tumor growth in human cervical cancers. J Interferon Cytokine Res. 2009; 29:695–703. [PubMed: 19642906]

22. Zhou AM, Zhao JJ, Ye J, Xiao WH, Kalvakolanu DV, Liu RY. Expression and clinical significance of GRIM-19 in non-small cell lung cancer. Ai Zheng. 2009; 28:431–5. [PubMed: 19622307]

23. Gong LB, Luo XL, Liu SY, Tao DD, Gong JP, Hu JB. Correlations of GRIM-19 and its target gene product STAT3 to malignancy of human colorectal carcinoma. Ai Zheng. 2007; 26:683–7. [PubMed: 17626740]

24. Zhang Y, Hao H, Zhao S, Liu Q, Yuan Q, Ni S, et al. Downregulation of GRIM-19 promotes growth and migration of human glioma cells. Cancer Sci. 2011; 102:1991–9. [PubMed: 21827581]

25. Hynes RO. Integrins: bidirectional, allosteric signaling machines. Cell. 2002; 110:673–87. [PubMed: 12297042]

26. Murphy DA, Courtneidge SA. The 'ins' and 'outs' of podosomes and invadopodia: characteristics, formation and function. Nature reviews Molecular cell biology. 2011; 12:413–26. [PubMed: 21697900]

27. Weed SA, Parsons JT. Cortactin: coupling membrane dynamics to cortical actin assembly. Oncogene. 2001; 20:6418–34. [PubMed: 11607842]

28. Buday L, Downward J. Roles of cortactin in tumor pathogenesis. Biochim Biophys Acta. 2007; 1775:263–73. [PubMed: 17292556]

29. Li X, Zheng H, Hara T, Takahashi H, Masuda S, Wang Z, et al. Aberrant expression of cortactin and fascin are effective markers for pathogenesis, invasion, metastasis and prognosis of gastric carcinomas. Int J Oncol. 2008; 33:69–79. [PubMed: 18575752]

30. Patel AS, Schechter GL, Wasilenko WJ, Somers KD. Overexpression of EMS1/cortactin in NIH3T3 fibroblasts causes increased cell motility and invasion in vitro. Oncogene. 1998; 16:3227–32. [PubMed: 9681820]

31. Li Y, Tondravi M, Liu J, Smith E, Haudenschild CC, Kaczmarek M, et al. Cortactin potentiates bone metastasis of breast cancer cells. Cancer Res. 2001; 61:6906–11. [PubMed: 11559568]

32. Yamada S, Yanamoto S, Kawasaki G, Mizuno A, Nemoto TK. Overexpression of cortactin increases invasion potential in oral squamous cell carcinoma. Pathol Oncol Res. 2010; 16:523–31. [PubMed: 20069395]

33. Theocharis S, Klijanienko J, Giaginis C, Alexandrou P, Patsouris E, Sastre-Garau X. FAK and Src expression in mobile tongue squamous cell carcinoma: associations with clinicopathological parameters and patients survival. J Cancer Res Clin Oncol. 2012; 138:1369–77. [PubMed: 22488171]

34. van Oijen MG, Rijksen G, ten Broek FW, Slootweg PJ. Overexpression of c-Src in areas of hyperproliferation in head and neck cancer, premalignant lesions and benign mucosal disorders. J Oral Pathol Med. 1998; 27:147–52. [PubMed: 9563568]

35. Chen JY, Hung CC, Huang KL, Chen YT, Liu SY, Chiang WF, et al. Src family kinases mediate betel quid-induced oral cancer cell motility and could be a biomarker for early invasion in oral squamous cell carcinoma. Neoplasia. 2008; 10:1393–401. [PubMed: 19048118]

36. Koppikar P, Choi SH, Egloff AM, Cai Q, Suzuki S, Freilino M, et al. Combined inhibition of c-Src and epidermal growth factor receptor abrogates growth and invasion of head and neck squamous cell carcinoma. Clin Cancer Res. 2008; 14:4284–91. [PubMed: 18594011]

37. Matsouka PT, Flier JS. Relationship between c-src tyrosine kinase activity and the control of glucose transporter gene expression. Molecular endocrinology. 1989; 3:1845–51. [PubMed: 2481817]

38. White MK, Rall TB, Weber MJ. Differential regulation of glucose transporter isoforms by the src oncogene in chicken embryo fibroblasts. Mol Cell Biol. 1991; 11:4448–54. [PubMed: 1875932]

39. Valle-Casuso JC, Gonzalez-Sanchez A, Medina JM, Tabernero A. HIF-1 and c-Src mediate increased glucose uptake induced by endothelin-1 and connexin43 in astrocytes. PloS one. 2012; 7:e32448. [PubMed: 22384254]

40. Koppenol WH, Bounds PL, Dang CV. Otto Warburg's contributions to current concepts of cancer metabolism. Nat Rev Cancer. 2011; 11:325–37. [PubMed: 21508971]

41. Jiang LQ, Feng X, Zhou W, Knyazev PG, Ullrich A, Chen Z. Csk-binding protein (Cbp) negatively regulates epidermal growth factor-induced cell transformation by controlling Src activation. Oncogene. 2006; 25:5495–506. [PubMed: 16636672]

42. Fearnley IM, Carroll J, Shannon RJ, Runswick MJ, Walker JE, Hirst J. GRIM-19, a cell death regulatory gene product, is a subunit of bovine mitochondrial NADH:ubiquinone oxidoreductase (complex I). J Biol Chem. 2001; 276:38345–8. [PubMed: 11522775]

43. Huang G, Lu H, Hao A, Ng DC, Ponniah S, Guo K, et al. GRIM-19, a cell death regulatory protein, is essential for assembly and function of mitochondrial complex I. Mol Cell Biol. 2004; 24:8447–56. [PubMed: 15367666]

44. Sena LA, Chandel NS. Physiological roles of mitochondrial reactive oxygen species. Mol Cell. 2012; 48:158–67. [PubMed: 23102266]

45. Giannoni E, Taddei ML, Chiarugi P. Src redox regulation: again in the front line. Free Radic Biol Med. 2010; 49:516–27. [PubMed: 20434540]

46. Suzuki K, Oneyama C, Kimura H, Tajima S, Okada M. Down-regulation of the tumor suppressor C-terminal Src kinase (Csk)-binding protein (Cbp)/PAG1 is mediated by epigenetic histone modifications via the mitogen-activated protein kinase (MAPK)/phosphatidylinositol 3-kinase (PI3K) pathway. J Biol Chem. 2011; 286:15698–706. [PubMed: 21388951]

47. Lindner DJ, Borden EC, Kalvakolanu DV. Synergistic antitumor effects of a combination of interferons and retinoic acid on human tumor cells in vitro and in vivo. Clin Cancer Res. 1997; 3:931–7. [PubMed: 9815768]
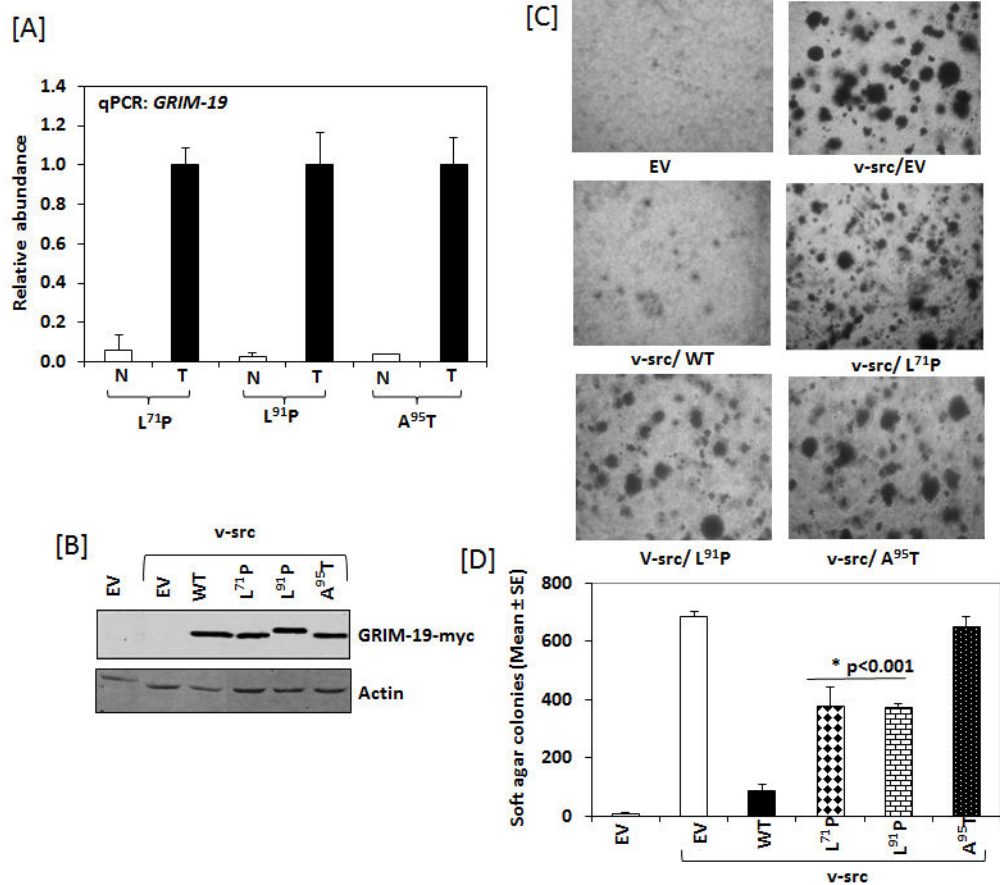
Figure 1.
A) Relative levels of *GRIM-19* in SCC and matched normal tissue by real-time PCR. Data presented are mean ± sd from three independent technical replicates of cDNA. B) Western blot analysis of Myc epitope-tagged GRIM-19 expression levels and actin in the indicated cell lines. C) SCC-derived *GRIM-19* mutants are poor at inhibiting v-Src-induced transformation. GRIM-19 mutants fail to inhibit anchorage-independent growth of v-Src-expressing 3Y1 cells. Soft-agar colonies formed were counted using an automated counter. D) Quantification of soft-agar colonies formed. Multiple non-overlapping fields in a well were counted. Data presented are Mean ± SD (*n* = 6). EV: empty control vector transfected cells with respect to v-Src. EV under v-Src refers to control vector (empty) transfected cells with respect to GRIM-19.
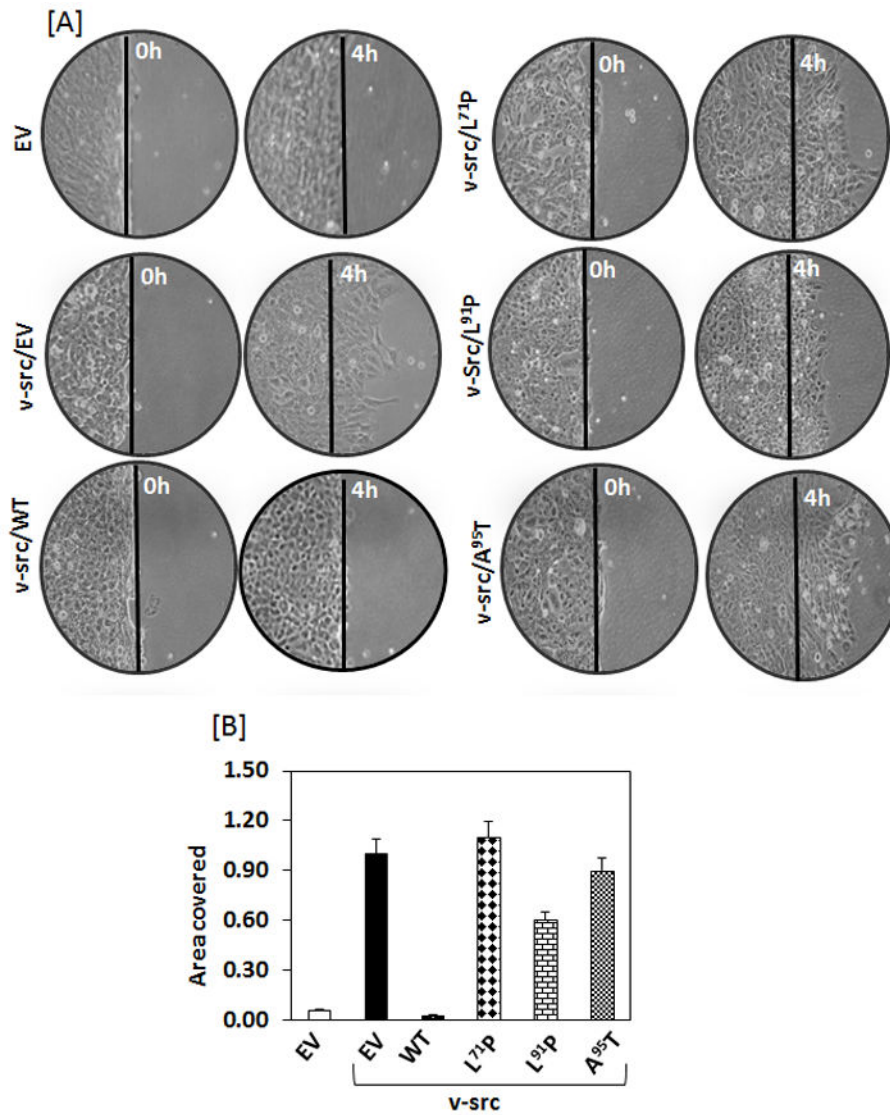
Figure 2.
SCC-derived GRIM-19 mutants lost their ability to inhibit v-Src induced cell motility. A) Wound-Scratch model was used to monitor the migration of cells into the denuded area. B) Quantitative representation of migration as percent of wound closed. Data represent Mean ± SE (n=6).
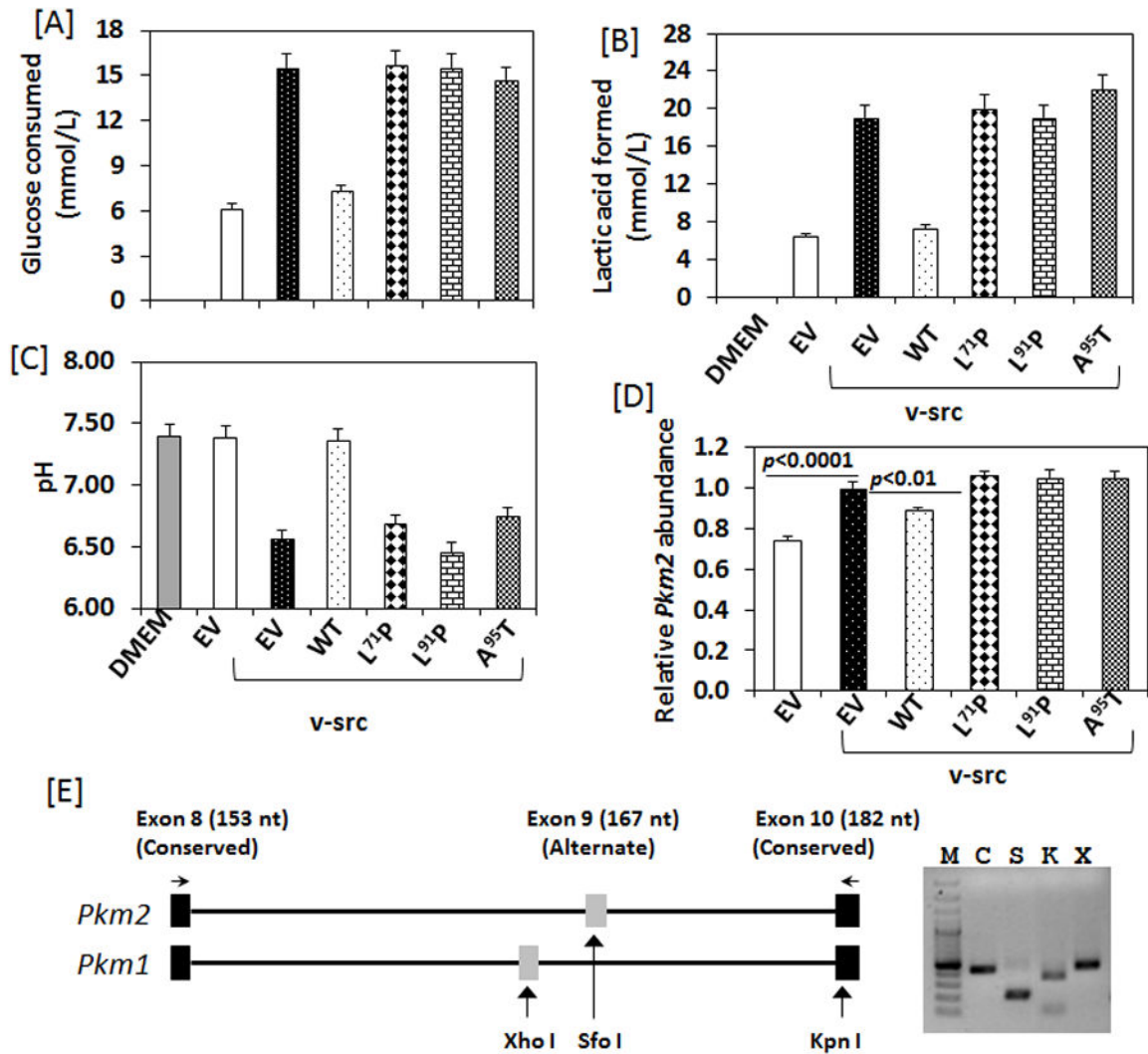
Figure 3.
Transformed 3Y1 cells exhibit Warburg effect similar to cancer cells. A–B) Metabolites present in spent medium were analyzed using Radiometer ABL-725 (Diamond Diagnostics, MA) as per the manufacturer's protocol. Residual glucose (presented as glucose consumed) and lactate levels were measured. Data represent Mean ± SE of two experiments (n=6). C) The pH of the spent medium at the end of the experimental period. D) Transcript levels of *Pkm2* in the indicated cell lines. No differences in *Pkm2* levels are apparent in the presence of mutants while wild-type GRIM-19 suppresses *Pkm2* levels compared to v-Src-expressing cells. E) Naïve and v-Src-transformed 3Y1 express only the *Pkm2* transcript. Primers (horizontal arrows) do not discriminate *Pkm1* or *Pkm2* transcripts. PCR products were digested with restriction enzymes (indicated with vertical arrows) to confirm their identity (Key: S – Sfo I, K – Kpn I, X – Xho I, C – Control and M – DNA marker).
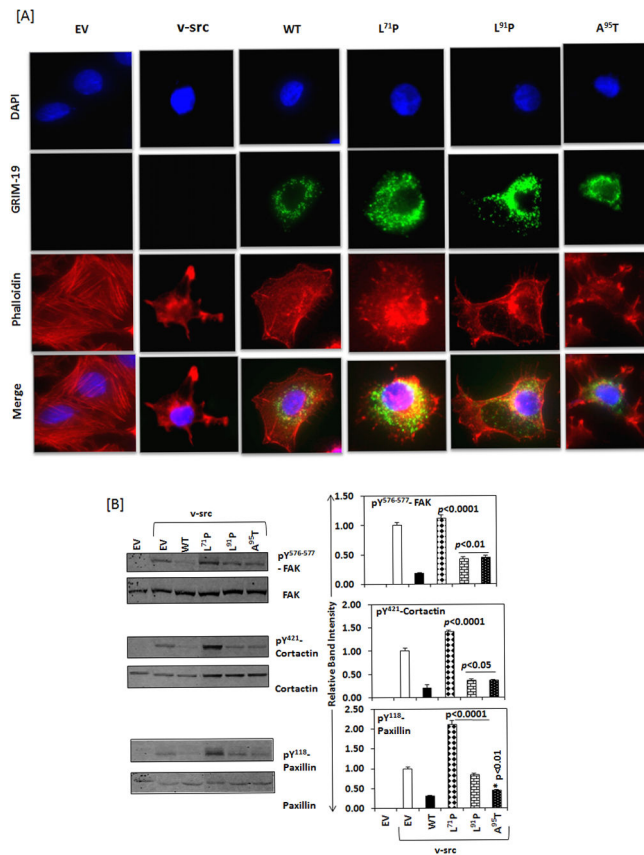
Figure 4.
SCC-derived *GRIM-19* mutants cannot revert completely the v-Src-induced transformed phenotype of 3Y1 cells. A) Immunofluorescent images of v-Src-expressing 3Y1 cell derivatives showing Myc-tagged GRIM-19 (Green), actin network (Red) and nucleus (Blue). Prominent stress fibers are seen in control 3Y1 cells (EV) while v-Src-expressing cells totally lack them. In cells expressing v-Src alone, dense actin staining is observed in podosome-like structures and stress fibers are completely absent. Wild-type GRIM-19 restores stress fibers while the mutants are unable to restore them like wild-type GRIM-19. B) Differential effect of SCC-derived GRIM-19 mutant proteins on v-Src kinase activity in 3Y1 cells. Semi-quantitative analysis of v-Src substrates in whole cell lysates prepared from adherent cells. Western blot profile of phosphorylated and total levels of the indicated proteins (left panels). Top panel: Tyrosines[576–577]-phosphorylated Fak levels are comparable in L[71]P mutant and v-Src-expressing cells. Data presented are mean ± SD ($n = 3$). Middle panel: Tyrosine[421]-phosphorylated cortactin levels are higher in L[71]P mutant than v-Src-expressing cells. Data presented are mean ± SD ($n = 5$). Bottom panel: Tyrosine[118]–phosphorylated paxillin levels are higher in L[71]P mutant than v-Src-expressing cells. Data presented are mean ± SD ($n = 3$). Quantified representation of Western blot data (phospho-protein over total protein levels) is presented to the right.
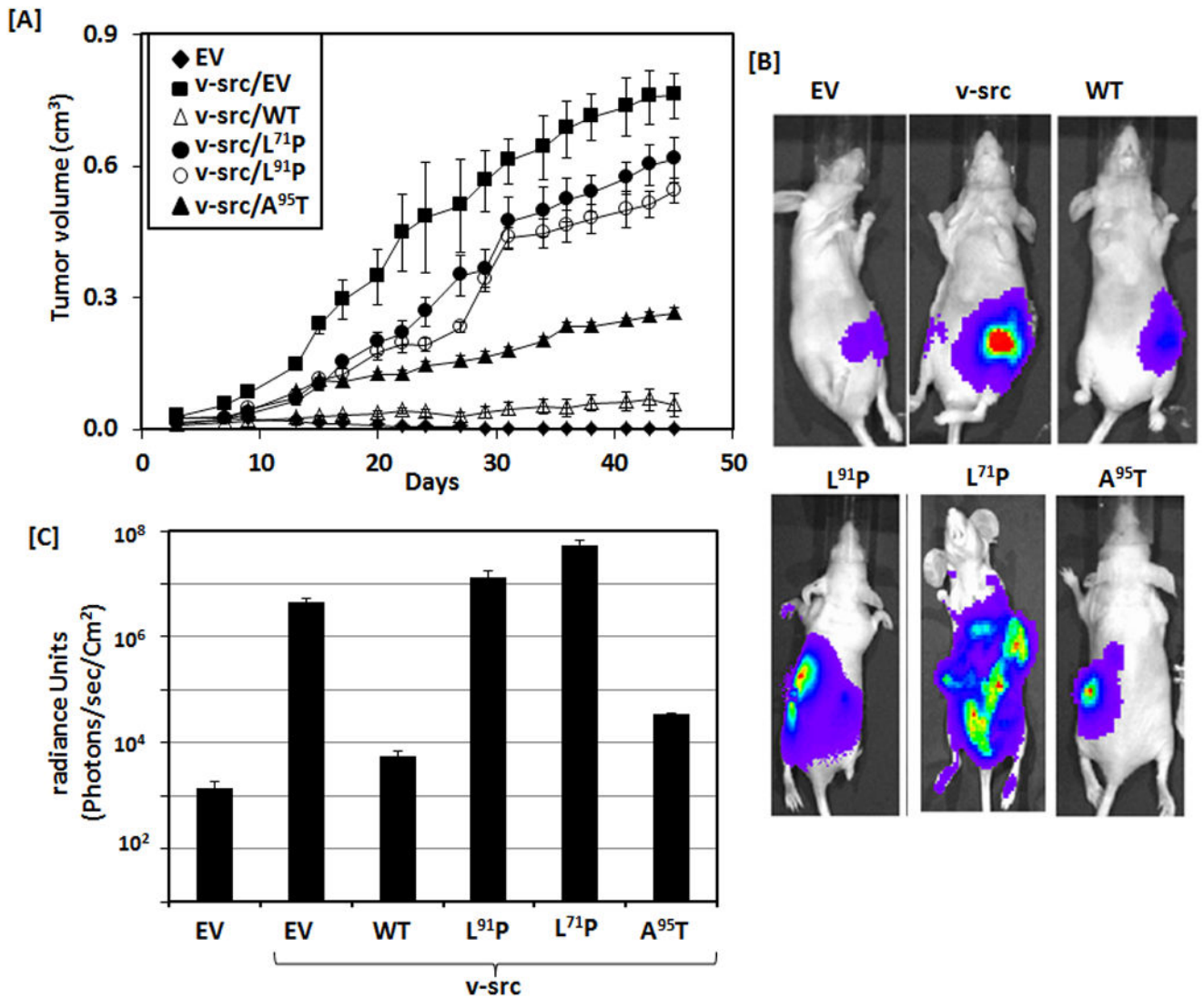
Figure 5.
Effects of GRIM-19 mutants on v-src driven tumor growth *in vivo.* A) Growth of tumor xenografts in athymic nude mice (n=10 mice/group). B) Metastatic spread of v-Src transformed cells in nude mice. 3Y1 cell lines were lentivirally transduced to express firefly luciferase to monitor their movement and growth. Light signals were captured after administering luciferin. Mutant cells expressing $L^{71}P$ and $L^{91}P$ showed aggressive spread of tumor-like 3Y1 cells while GRIM-19 wild type and $A^{95}T$ mutant showed only a localized spread. Image acquisition settings were as follows: Bin 8, FOV25, f1, 30sec exposure, background subtracted, flat-fielded, cosmic. C) Quantification of tumor spread. Data represent mean ± SE (n=4 mice/group). The differences between WT and $A^{95}T$ are statistically significant (*p*<0.02).
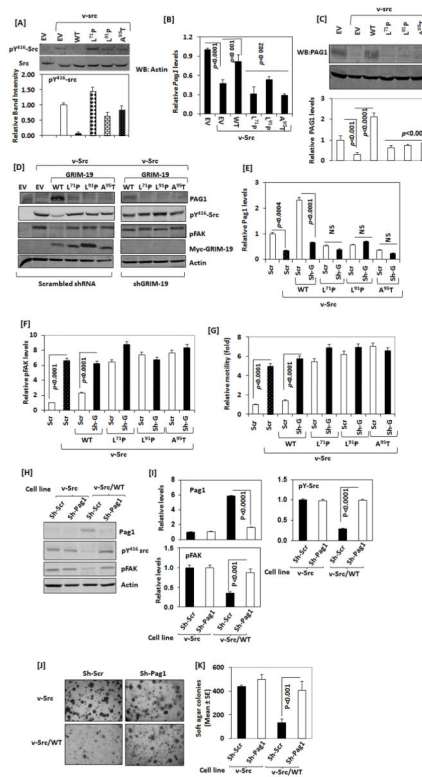
Figure 6.

Regulation of the v-src activity by GRIM-19. A) Active Src levels in the indicated 3Y1 cell lines by Western blot. Tyrosine[416]-phosphorylated Src levels in the presence of wild-type GRIM-19, while the mutant-expressing cells have a higher level of active Src and this difference is not reflected in total Src protein levels. Data presented are mean ± SE (*n* = 7). B) Relative *Pag1* transcript abundance as determined by qPCR; and C) Pag1 protein levels in the indicated cell lines. The bar graph shows the quantified data of Pag 1 protein. D) RNA*i*-mediated knockdown of GRIM-19 results in a restoration of v-src activity *via* a repression of Pag1 levels. Scr: scrambled shRNA control; sh-G: shRNA specific for GRIM-19. Note the upregulation of src activity (pY416) and an increase in FAK phosphorylation following GRIM-19 knockdown. E&F) show the quantification of Pag1 and pFAK levels. Data presented are mean ± SE (*n* = 4). G) Transwell migration assay. 3Y1 cell lines expressing various GRIM-19 mutants in the absence/or presence of shRNA-specific for GRIM-19 were used for cell invasion through membranes using a commercially available kit (Invitrogen, Inc). Data represent mean ± SE (*n* = 6). H) RNA*i*-mediated knockdown of Pag1 relieves GRIM-19 mediated inhibition of src-activity. sh-Scr: scrambled shRNA control; sh-Pag1: Pag1-specific shRNA. After transducing cells with lentiviral expression vector carrying the indicated shRNAs stable cell populations were isolated. Lysates were subjected to Western blotting with the indicated antibodies. I) Relative levels of Pag1, pFAK and pY-Src following Pag1 knockdown. Western blot data from 3 separate blots were quantified and presented. *p* values were indicated where significant. J&K) Impact of Pag1 knockdown on soft-agar colony formation. J) Photomicrographs of representative samples.

K) Quantification of soft-agar colony formation. Data represent mean ± SE (n = 5 plates/cell line). p values were indicated where significant.